ADVANCED FUNCTIONAL MATERIALS
www.afm-journal.de

Graphene Oxide-Cyclic R10 Peptide Nuclear Translocation Nanoplatforms for the Surmounting of Multiple-Drug Resistance

Zhaoxu Tu, Ievgen S. Donskyi, Haishi Qiao, Zhonglin Zhu, Wolfgang E. S. Unger, Christian P. R. Hackenberger, Wei Chen, Mohsen Adeli,* and Rainer Haag**

Multidrug resistance resulting from a variety of defensive pathways in cancer has become a global concern with a considerable impact on the mortality associated with the failure of traditional chemotherapy. Therefore, further research and new therapies are required to overcome this challenge. In this work, a cyclic R10 peptide (cR_{10}) is conjugated to polyglycerol-covered nanographene oxide to engineer a nanoplatform for the surmounting of multidrug resistance. The nuclear translocation of the nanoplatform, facilitated by cR_{10} peptide, and subsequently, a laser-triggered release of the loaded doxorubicin result in efficient anticancer activity confirmed by both in vitro and in vivo experiments. The synthesized nanoplatform with a combination of different features, including active nucleus-targeting, high-loading capacity, controlled release of cargo, and photothermal property, provides a new strategy for circumventing multidrug resistant cancers.

1. Introduction

Cancer-related death, which is one of the most terrible killers around the world, will rise to around 150 million by 2020.[1] The development of safer and more effective tumor treatment tactics is urgent but still formidable.[2,3] Graphene, as the most widely used 2D nanomaterials, has shown extraordinary performance in the antitumor nanomedicine exploitation,[4–6] which is attributed to its stability, photothermal property, high loading capacity, fast cellular uptake, and biodegradability.[7–13] Although many graphene-based antitumor systems have been constructed and much progress has been achieved in this field, the situation becomes more complicated and challenging when it meets the multidrug resistance (MDR).[14,15] The emergence of MDR is largely owing to the overexpression of ATP-binding cassette, in particular, P-glycoprotein (P-gP), on the plasma membrane.[14–16] These proteins reduce the internalization of therapeutic agents into the cells and even mediate the efflux of these agents from the cells. In recent years, a variety of functional nanomaterials and smart nanodevices were developed to incapacitate P-gP and to deliver anticancer drugs across the plasma membrane.[16,17] Despite the efficient cellular uptake and improved drug concentration inside the cytoplasm of cancer cells, the "efflux pump" still frustrates the chemotherapy.[14–16] This shortage is more serious when it comes to therapeutic agents with specific targeting organelles, such as doxorubicin (DOX), whose anticancer mechanism is to intercalate with DNA in the nucleus.[18,19] Therefore, efficient tumor therapy could hardly be achieved if MDR is not efficiently suppressed and therapeutic agents are not localized into the target organelles.[18,19]

Recently, nucleus-targeting strategies were proposed for the chemotherapy of MDR tumors by DOX.[20] By this strategy, DOX

Dr. Z. Tu, Dr. H. Qiao, Z. Zhu, Prof. W. Chen
Department of Pharmaceutical Engineering
School of Engineering
China Pharmaceutical University
Nanjing 210009, China
E-mail: w.chen@cpu.edu.cn

Dr. Z. Tu, Dr. I. S. Donskyi, Prof. M. Adeli, Prof. R. Haag
Institut für Chemie und Biochemie
Freie Universität Berlin
Takustr. 3, Berlin 14195, Germany
E-mail: aadeli@fu-berlin.de; haag@chemie.fu-berlin.de

The ORCID identification number(s) for the author(s) of this article can be found under https://doi.org/10.1002/adfm.202000933.

DOI: 10.1002/adfm.202000933

Dr. I. S. Donskyi, Dr. W. E. S. Unger
BAM – Federal Institute for Material Science and Testing
Division 6.1
Surface Analysis and Interfacial Chemistry
Unter den Eichen 44–46, Berlin 12205, Germany

Prof. C. P. R. Hackenberger
Department of Chemical Biology
Leibniz-Forschungsinstitut für Molekulare Pharmakologie (FMP)
Robert-Rössle-Strasse 10, Berlin 13125, Germany

Prof. C. P. R. Hackenberger
Humboldt Universität zu Berlin
Institut für Chemie
Brook-Taylor-Str. 2, Berlin 12489, Germany

Prof. M. Adeli
Department of Chemistry
Faculty of Science
Lorestan University
Khorramabad 68151-44316, Iran

could be delivered into nucleus and the "efflux pump" on the plasma membrane could be hopefully avoided. Arginine-rich cell-penetrating peptides (CPPs), particularly the TAT peptide, which originates from the HIV-1 virus, are shown to be efficient vectors to translocate nanoparticles including mesoporous silica nanoparticles,[21,22] upconversion nanoparticles,[23] copper sulfide nanoparticles,[24] and polymer nanoparticles[25,26] into the cell nucleus. Cyclization of CPPs has been demonstrated as a new strategy to improve their ability as transmembrane carriers and nucleus targeting agents.[27–31] For example, cyclic TAT (cTAT) has been proven to show higher ability to facilitate the cellular translocation of proteins than linear TAT at 4 °C.[30] The internalized cTAT-decorated protein is distributed both in the cytoplasm and in the nucleolus, a nuclear compartment.[30] Moreover, cyclic R10 peptide (cR_{10}) even has displayed higher transduction location efficacy than cTAT.[32] Accordingly, cR_{10} peptide is supposed to be an effective molecule for the nuclear targeting and translocation of nanocarriers into cells.[32]

Furthermore, the size of nanoparticles restricts their ability to enter the cellular nucleus.[33,34] In general, nanoparticles bigger than 40 nm can scarcely cross the nuclear membrane.[20,33,34] Graphite could be exfoliated to small sheets, 15–30 nm, via intensified oxidation processes.[35,36] The obtained nanographene oxide (nGO) contains a large number of epoxy and hydroxyl functional groups on the basal plane and carboxyl on its edges.[36] Moreover, hyperbranched polyglycerol (hPG) with great potential in a wide range of biomedical applications, including drug delivery, tissue engineering, and pathogen interactions,[37,38] has been used to improve the biological safety and performances of nanomaterials, such as graphene.[39–41]

In this work, we have synthesized polyglycerol-functionalized nGO derivatives with the ability of the intra-nucleus delivery and release of antitumor therapeutic agents and MDR suppression (**Figure 1**). nGO with a 15–30 nm average size was produced and functionalized by hPG via an amidation reaction. Subsequently, cR_{10} peptide was conjugated to the residual amino groups of hPG and DOX was loaded onto the nGO sheets by noncovalent interactions. While hPG and cR_{10} peptide improved the biocompatibility and nuclear internalization of nGO sheets, respectively, laser irradiation triggered the intra-nucleus release of DOX from the carrier. Both in vitro and in vivo results have demonstrated the successful overcoming of the MDR and improved antitumor effect of the loaded DOX.

2. Results and Discussion

2.1. Synthesis of the cR_{10}-Functionalized Polyglycerol-Covered Nanosheets

nGO was produced according to the reported procedure in literature.[35] hPG with 10% amino functional groups ($hPG(NH_2)_{10\%}$) was prepared via an azido substitution and reduction procedure from hPG.[15] Then, the $hPG(NH_2)_{10\%}$ was conjugated onto nGO via an amidation reaction with 1-ethyl-3-(3-dimethylaminopropyl)carbodiimide hydrochloride (EDC. HCl) as condensing agent in 2-(*N*-morpholino)ethanesulfonic acid solution (MES) to obtain hPG-covered nGO (GOP).[15] Afterward, (bicyclo[6.1.0]non-4-yn-9-yl)methyl 4-nitrophenyl carbonate (BCN) was applied to modify GOP with cyclooctyne moieties to produce GOP_{BCN}.[42] The reaction between thiol group of cR_{10} peptide and cyclooctyne moieties of GOP_{BCN} in PBS resulted in nanoplatforms with the peptide functionality (GOPR) (**Scheme 1**).[43] Detailed information about the synthesis and characterizations of GOPR can be found in the Supporting Information.

TEM images showed the average size of nGO was around 17 nm (**Figure 2**A), while the value slightly increased after covering by hPG and conjugation of peptides (Figure 2B,C). The small average size (20 nm) is a significant factor that can affect the cellular uptake and nucleus localization of GOPR.

The composition of nGO, GOP, and GOPR was investigated by X-ray photoelectron spectroscopy (XPS), UV-vis absorption, and thermogravimetric analysis (TGA). In Figure 2D, the C1s component peak at 284.6 eV is assigned to sp^2 hybridized

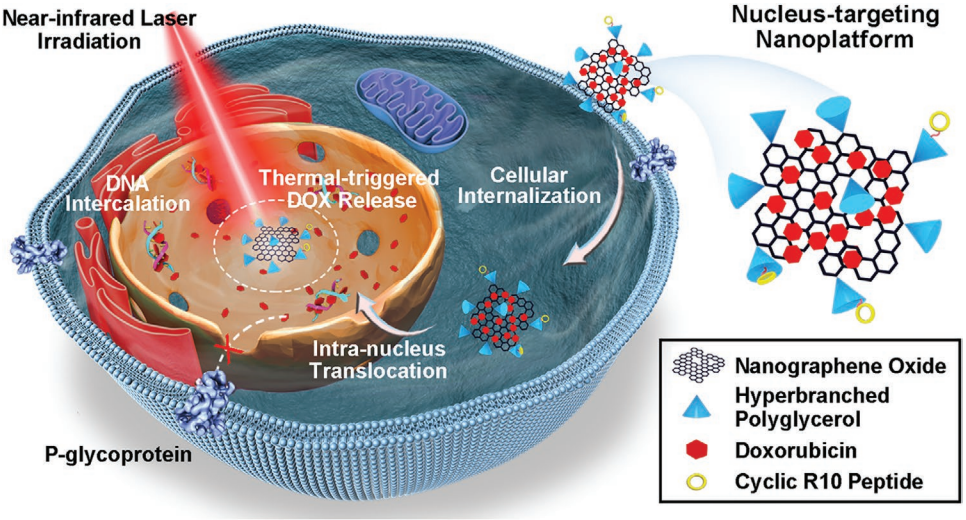

Figure 1. Suppression of MDR by polyglycerol-covered nGO sheets. After efficient uptake by the tumor cells, nanosheets localize inside the nucleus by cR_{10} peptide. Consequently, an intra-nucleus release of DOX triggered by NIR irradiation resulted in efficient chemophototherapy against MDR tumors.

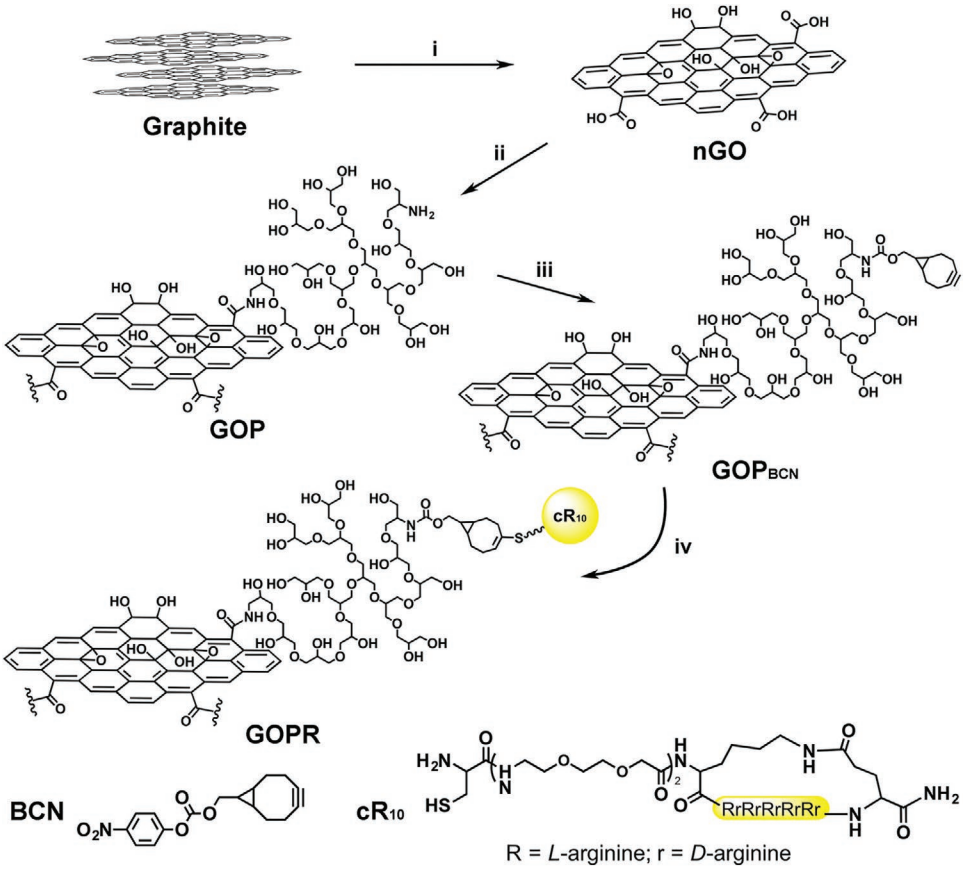

Scheme 1. Synthesis routes for the production of nGO, GOP, and GOPR. Detailed information for step i, ii, iii, and iv are as follow: i) dispersed in mixture (v/v = 3:1) of H_2SO_4 (98%) and HNO_3 (65%), 120 °C, 2 d; ii) with $hPG(NH_2)_{10\%}$, dispersed in MES solution including EDC.HCl, room temperature (RT), overnight; iii) with BCN, dispersed in dimethylformamide (DMF) including triethylamine (TEA), RT, overnight; iv) with cR_{10} peptide, dispersed in PBS (7.4), RT, overnight.

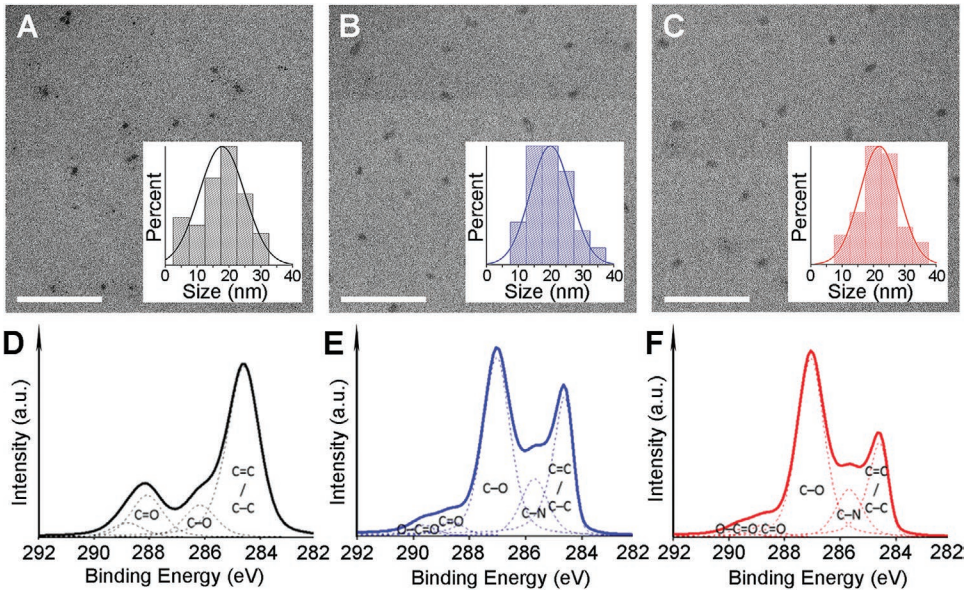

Figure 2. The TEM images and size profiles of A) nGO, B) GOP, and C) GOPR nanomaterials. The scale bars correspond to 200 nm. The highly resolved C1s XPS spectrum of D) nGO, E) GOP, and F) GOPR nanomaterials.

carbon bonds of the graphene platform. Component peaks at 286.2 and 288.1 eV were attributed to C—O and C=O bonds created after oxidation of graphite. This result confirmed the disruption of the plane and edges of graphene and formation of a large number of carbonyl, hydroxyl, carboxyl, and epoxy functional groups upon oxidation (Figure 2D). C1s XPS spectra of GOP and GOPR showed successful stepwise conjugation of hPG and cR_{10} peptide to the nGO. (Figure 2E,F, Table S1, Supporting Information). The appearance of C—N bond related component peaks in the survey spectra of GOP and GOPR were attributed to the amino groups, amide groups, and guanidine groups in $hPG(NH_2)_{10\%}$ and cR_{10}. In order to confirm the reaction between the thiol group of cR_{10} and GOP_{BCN}, a control reaction was performed. Accordingly, cR_{10} without thiol functional group was incubated with GOP_{BCN} and the product of the reaction was characterized by XPS. Significant changes in the XPS spectrum of the product were not found, which indicated that peptide was not conjugated to the graphene sheets (Table S2, Figures S1 and S2, Supporting Information). This control reaction proved the critical role of thiol group for the conjugation of cR_{10} to GOP_{BCN}.

The composition of the synthesized nanomaterials, as well as their peptide contents, were further investigated by UV–vis experiments. They showed a characteristic absorption peak at 225 nm, which was used to determine the concentration of nGO in the aqueous solutions (Figure S3A, Supporting Information). According to these UV–vis experiments, the nGO and hPG contents of GOP were around 46% and 54%, respectively. After conjugation of cR_{10} peptide to GOP, the nGO decreased to around 43.8%, indicating around 4.8% peptide content for GOPR (Figure S3B, Supporting Information). Data related to the composition of nanomaterials can be found in Supporting Information, page 9.

2.2. Cellular Uptake and Intracellular Distribution

The characterized materials were used for the cell experiments, including cytotoxicity and intra-nucleus localization. According to Cell Counting Kit-8 (CCK-8) assays, the toxicity of GOP and GOPR against multidrug-resistant HeLa (HeLa-R) cells was negligible up to 300 μg mL^{-1} (Figure S5, Supporting Information). The low toxicity of these nanomaterials holds promise for biomedical applications. Therefore, we labeled the nanomaterials by fluorescein isothiocyanate (FITC) (Figure S6, Supporting Information) and investigated their uptake by HeLa-R cells using confocal laser scanning microscopy (CLSM) (**Figure 3**A,B) and fluorescence-activated cell sorting (FACS) (Figure 3C). GOP showed very low cellular uptake after 6 h incubation due to the hPG coverage.[40] However, GOPR was efficiently taken up by HeLa-R cells, indicating a significant role for cR_{10} in the cellular internalization of functionalized nanosheets (Figure 3B). The quantitative data obtained by FACS showed an increase in the

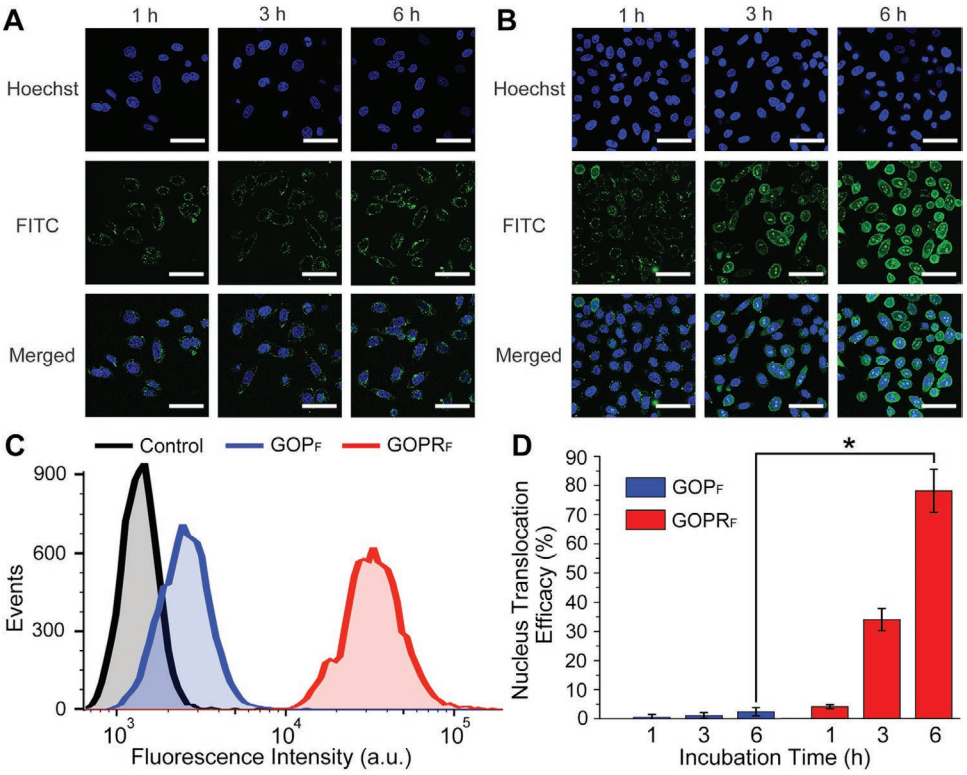

Figure 3. The CLSM images of living HeLa-R cells incubated with A) FITC-labeled GOP (GOP_F) and B) FITC-labeled GOPR ($GOPR_F$) for 1, 3, and 6 h, respectively. Scale bars correspond to 50 μm. C) FACS results for HeLa-R cells after 6 h incubation with GOP_F and $GOPR_F$. HeLa-R cells without any treatments were applied as a control. D) CLSM-based statistical analysis of the nucleus translocation efficacy for the HeLa-R cells incubated with GOP_F and $GOPR_F$ for 1, 3, and 6 h. Mean ± SD. ($n = 3$, Student's t-test, $^*p < 0.0001$).

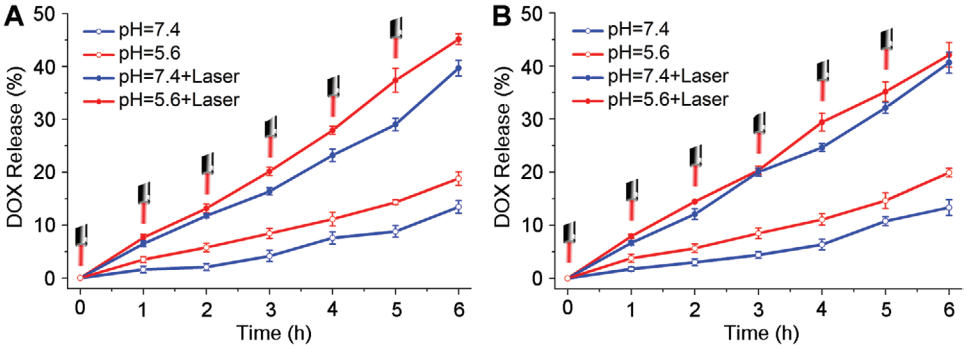

Figure 4. In vitro release profiles of DOX from the A) GOP_D and B) $GOPR_D$ at 37 °C under various conditions. NIR laser irradiation (808 nm, 0.5 W cm^{-2}) was applied 5 min every 1 h. Mean ± SD (n = 3).

uptake efficiency ten times after conjugation of cR_{10} peptide to nanosheets (Figure 3C).

It has been shown that conjugation with cyclic cell-penetrating peptides (cCPPs) like cR_{10} or cTAT enhanced the transduction of protein-cargo in living cells.[30,32] Additionally, non-cleavable cCPP conjugates have shown the ability to accumulate in the nucleoli within the nucleus.[32] Along these lines, we proposed that the conjugation of cR_{10} peptide to nanomaterials is effective for the nuclear localization of their cargos. Interestingly, the intra-nucleus translocation of GOPR was very efficient and cR_{10} was able to facilitate the localization of nanosheets inside the nucleus (Figure 3B). Statistical analysis was applied to calculate the percent of the cells with nucleus-translocated graphene sheets (Figure 3D). While localization of GOP into the nucleus of cells after 6 h incubation was negligible, GOPR was effectively transferred into the nucleus and around 80% of cells affected by the nucleus-targeting peptide.

2.3. Preparation of DOX-Loaded Nanosheets and Their Release Profiles

The action site of DOX is inside of the nucleus, where it inhibits the macromolecular biosynthesis of DNA and causes apoptosis of carcinoma cells.[18,19] Therefore, translocation of this therapeutic agent inside the nucleus, after cellular internalization, is a crucial step. However, many nanocarriers discharge DOX molecules in the cytoplasm, which causes failure of chemotherapy against MDR cells.[14,16,17]

cR_{10} peptides with the ability of driving the nanosized graphene sheets into nucleus are supposed to facilitate the localization of their cargo, DOX molecules, inside this compartment. DOX-loaded GOP and GOPR (GOP_D and $GOPR_D$, respectively) were prepared according to reported methods.[44] The loading capacities of GOP_D and $GOPR_D$ were calculated to be 12.5% (w/w%) and 11.7% (w/w%), respectively. The lower loading capacity of GOP_D and $GOPR_D$, in comparison with the reduced GO derivatives, was assigned to the disrupted graphene basal plan and limited sites for the efficient hydrophobic and π-π interactions with DOX molecules.[44] However, the loading capacity was still higher than most of the polymer-based nanocarriers.[45]

The photothermal effect is an unique characteristic for the graphene-based nanomaterials,[8,46] which is also beneficial for the controlled release of their cargo.[47,48] GOP and GOPR solutions at different concentrations were irradiated with the near-infrared (NIR) laser and the temperature variations were recorded (Figure S7, Supporting Information). After 10 min irradiation, the temperature of the aqueous solutions of GOP and GOPR (1 mg mL^{-1}) increased to 50 °C, which was enough for triggering the release of their cargo as well as an efficient photothermal therapy.[8,15] The ability of laser irradiation to accelerate the release of DOX from GOP_D and $GOPR_D$ was investigated at pH 5.6 and 7.4 (**Figure 4**). As expected, the release rate increased upon NIR laser irradiation, which was ascribed to the increased temperature of the nanosheets.[15] However, the effect of pH on the release rate of DOX from graphene sheets was not significant. This is an advantage for this system, because it results in a minimum leaking of drugs in the cytoplasm, optimum nucleus localization, and laser-triggered release of DOX. These spatiotemporally controlled release properties are very helpful for precise tumor therapy and to mitigate the unwanted side effects.[49,50]

2.4. DOX Cellular Uptake and Antitumor Effect

GOP_D and $GOPR_D$ were incubated with HeLa-R cells for 12 h to investigate the intracellular DOX release and distribution. The cells were irradiated with NIR laser (808 nm, 0.5 W cm^{-2}) for 10 min after 6 h incubation and non-irradiated cells were used as control. For the DOX.HCl-incubated HeLa-R cells, a significant difference between the irradiated and non-irradiated cells was not observed (**Figure 5**A). In both cases, the amount of DOX inside the cells and its therapeutic effect against cancer cells was low. The half maximal inhibitory concentration (IC50) value for DOX.HCl against HeLa-R cells with and without laser irradiation was 18.6 and 20.9 μg mL^{-1}, respectively (Figure 5C,D). The resistance of HeLa-R cells against DOX is due to many factors, especially overexpressed P-gP on the plasma membrane as efflux pumps.[14,15]

The DOX signal in GOP_D-treated cells, before and after laser irradiation, was similar to free DOX (Figure 5A). The reason for weak DOX signal is either low uptake of this drug or the lack of targeting ligand in GOP_D and localization in the cytoplasm, where most of the released DOX molecules were "pumped" into the external cellular environment. However, the IC50 value for the cells incubated with GOP_D

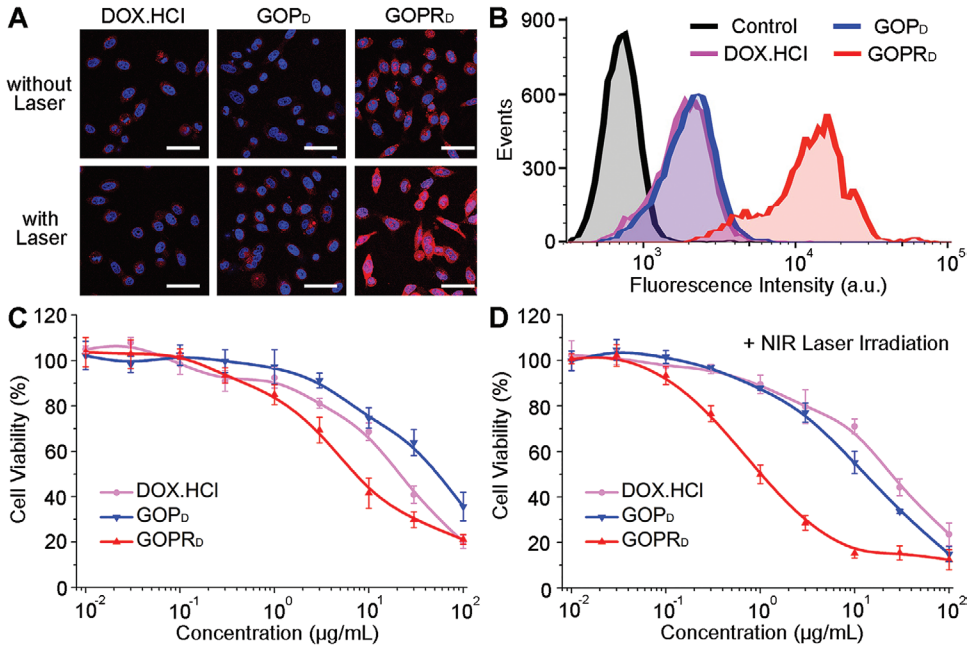

Figure 5. A) CLSM images of HeLa-R cells after 12 h incubation with DOX.HCl, GOP_D, and $GOPR_D$. For the experiments in the second row, cells were irradiated by NIR laser (808 nm, 0.5 W cm^{-2}) for 10 min after 6 h incubation. Scale bars correspond to 50 μm. B) FACS results for HeLa-R cells incubated with DOX.HCl, GOP_D, and $GOPR_D$ after 12 h. NIR laser (808 nm, 0.5 W cm^{-2}) irradiation was performed for 10 min after 6 h incubation. Anticancer efficacy of DOX.HCl, GOP_D, and $GOPR_D$ after 24 h incubation with HeLa-R cells C) without and D) with laser irradiation. Cells were irradiated by NIR laser (808 nm, 0.5 W cm^{-2}) for 10 min after 6 h incubation. Mean ± SD ($n = 3$).

reduced from 50.1 to 12.3 μg mL^{-1} after laser irradiation (Figure 5C,D). The enhanced therapeutic effect was attributed to the photothermal effect of nGO sheets and promoted release of therapeutic agents. Laser irradiation of cells treated with $GOPR_D$ resulted in a high DOX signal in nucleus, indicating the efficient nucleus translocation by cR_{10} peptide (Figure 5A). Before irradiation, the signal of DOX was weak, because its fluorescence was partially quenched by nGO sheets (Figure S9, Supporting Information).[15,44] This result confirmed that DOX molecules were majorly associated with nGO, and they were not considerably released during their journey inside the cytoplasm. The low IC50 of $GOPR_D$ without laser irradiation (9.4 μg mL^{-1}) is another proof for the successful targeting of this carrier and associating cargo with the carrier until nucleus internalization (Figure 5C). The IC50 of $GOPR_D$ plummeted to 1.1 μg mL^{-1} when NIR laser was employed. The high DOX content of the $GOPR_D$-treated cells (Figure 5B) and high therapeutic effect of this carrier (Figure 5D) proved the incapacity of MDR cells to discharge released DOX molecules into the external cellular environment after nuclear localization. From the in vitro studies, it can be concluded that the cR_{10}-functionalized graphene sheets were able to efficiently circumvent the MDR, due to the combination of a series of unique physicochemical and biological properties.

2.5. Biodistribution and Photothermal Effect

Although promising therapeutic effects were obtained in vitro, they cannot afford an efficient nGO-based nucleus-targeting and anticancer ability in vivo. However, the hPG coverage of the sheets decreases their unspecific interactions with the biosystems and effectively relieves the possible injuries,[15] which was reported for the bare graphene-treated animals.[51] Nanocarriers were labeled with 1,1′-bis(4-sulfobutyl) indodicarbocyanine-5-carboxylic acid (IDCC, a derivative dye of Cy5), and their biodistribution was studied. The labeled carriers were injected into the HeLa-R tumor-bearing nude mice. Mice were sacrificed after 24 h, and their tumors and main organs were isolated. The fluorescence intensities were measured quantitatively (**Figure 6**B and Table S3, Supporting Information). The fluorescence signal in tumors was stronger than other organs, such as liver and kidney, confirming an effective tumor localization of carriers. Interestingly, the accumulation of GOPR in tumors and organs was higher than GOP, which may have been attributed to the higher cellular internalization efficacy of this system.

In addition to triggering the release of the cargo, laser can induce a photothermal effect of nGO sheets, which improved the anticancer efficacy of these systems synergically.[8] In order to investigate the photothermal effect of carriers, saline, DOX.HCl, GOP_D, and $GOPR_D$ were intravenously administrated into nude mice. After 24 h, the NIR laser (808 nm, 0.5 W cm^{-2}) irradiation was applied in the tumor sites, and tumor local temperature was monitored with a thermal camera. While the tumor temperature of the saline- and DOX.HCl-treated mice increased from 30 to 37 °C, it reached 44.9 and 48.6 °C for GOP_D- and $GOPR_D$-treated mice, respectively (Figure 6A). This temperature range is reported to show an effective photothermal effect.[7,8]

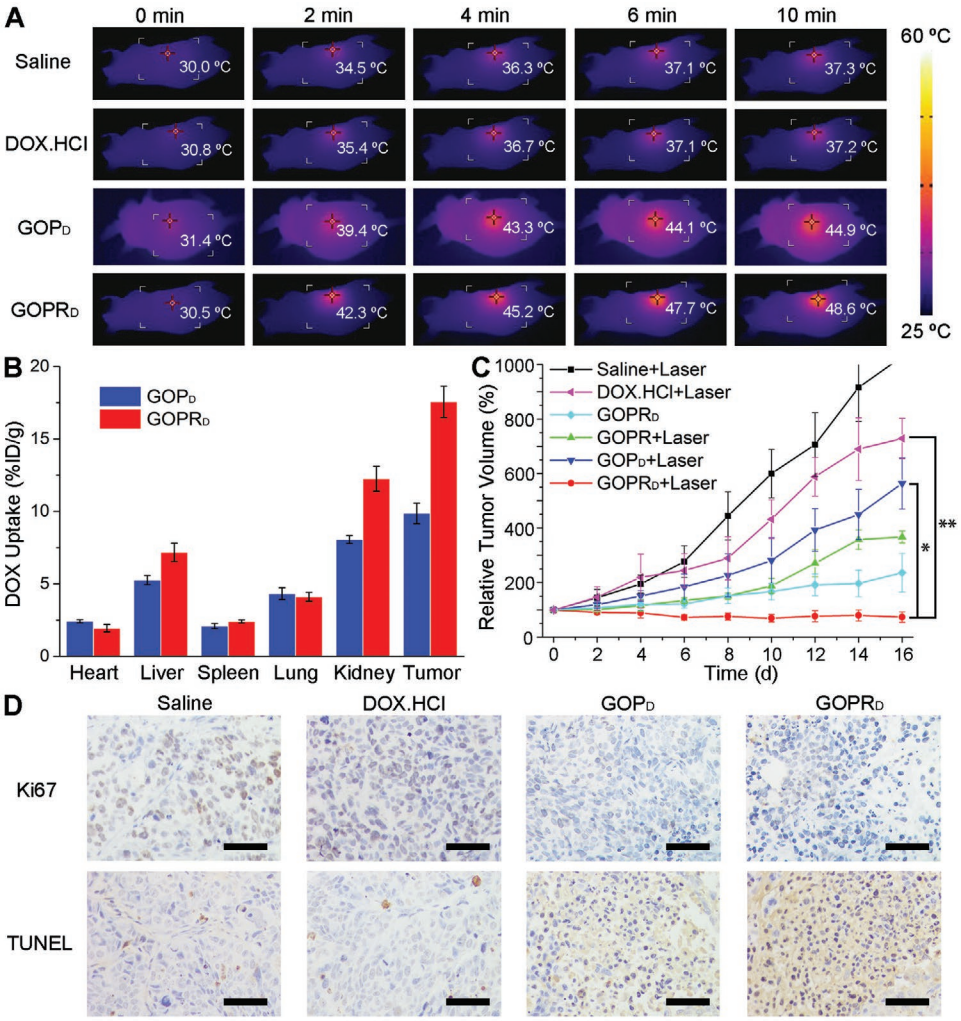

Figure 6. A) Thermographic images of HeLa-R tumor-engrafted nude mice after treatment with saline, DOX.HCl, GOP_D, and $GOPR_D$. The tumors were irradiated by NIR laser (808 nm, 0.5 W cm^{-2}) for 10 min. B) Quantitative calculation of in vivo DOX biodistributions in different organs and tumors of the nude mice 24 h after intravenous injection. C) The tumor volumes of HeLa-R tumor engrafted nude mice after treatment with saline 1), DOX.HCl 2), $GOPR_D$ 3), GOPR 4), GOP_D 5), and $GOPR_D$ 6). The tumors of mice in groups 1, 2, 4, 5, and 6 were irradiated with NIR laser (808 nm, 0.5 W cm^{-2}) for 10 min. Each nude mouse was intravenously administered at a dose of 5 mg kg^{-1} (DOX/body weight) at the beginning of this therapy. (*$p < 0.0001$; **$p < 0.00001$). D) Immunohistochemical analysis for HeLa-R tumors. Positive staining cells in Ki67 and TUNEL analysis are with a brown color. Scale bars correspond to 250 μm.

2.6. In Vivo Anticancer Effect

The tumor size (Figure 6C) and body weight (Figure S12, Supporting Information) were recorded in the following 16 days after treatment. The tumors of saline- and DOX.HCl-treated mice grew very fast, and DOX.HCl alone only exhibited limited tumor suppression. In the case of GOP_D-treated mice, the antitumor efficacy slightly improved but still was far away from satisfaction, even with irradiation. This was due to the low uptake efficacy and intra-cytoplasm release of drug, as well as its moderate photothermal effect. However, $GOPR_D$ showed much higher antitumor efficacy even without laser irradiation, and the tumor size was only 32.4% compared with the DOX.HCl-treated mice. This could be attributed to the efficient cR_{10} targeting and intra-nucleus release of the loaded DOX molecules. The most exciting therapeutic results came from the combination of $GOPR_D$ and laser irradiation at the tumor sites. The tumors kept shrinking during the whole treatment (the tumor size was only 10.1% compared with the DOX.HCl-treated mice after the therapy), which indicated the rational strategy to conquer MDR tumors.

The adverse side effects, including hair loss, bone marrow suppression, inflammation of the mouth, and other things, are always the concern of DOX when it is applied for clinical patients.[52] Body weight as the most representative indicator, was recorded to analyze the side effects of $GOPR_D$ (Figure S12, Supporting Information). It could be seen that the weight loss for the DOX.HCl-injected mice was quite apparent, particularly in the initial treatment stage. In addition, obvious diseased regions could be found in the heart histological staining of DOX.HCl-treated mice, indicating its serious cardiotoxicity (Figure S13, Supporting Information). These side effects could

rarely be observed in the GOP_D- and $GOPR_D$-treated mice, confirming the low side effects of these nanocarriers.

In order to investigate the antitumor therapeutic mechanism of these nucleus-targeting nanosheets, histological staining analyses were applied to the isolated tumors, including hematoxylin and eosin (H&E),[53] Ki67,[54] and TUNEL.[55] Compact tumor tissue was found for saline- and DOX.HCl-treated mice, while a remarkable reduction of tumor cells and more vacancies were observed after $GOPR_D$ administration (Figure S13, Supporting Information). Furthermore, less Ki67-positive cells (proliferative cells) and more TUNEL-positive cells (apoptotic cells) could be found in the $GOPR_D$-treated tumors (Figure 6D). On contrary, more proliferative tumor cells and less apoptotic tumor cells were observed in the case of saline- and DOX.HCl-treated mice (Figure 6D). These results confirmed the successful antitumor therapy by nucleus-targeting graphene-based nanoplatforms.

3. Conclusion

We demonstrated that the MDR in cancer could be successfully bypassed both in vitro and in vivo by nucleus targeting polyglycerol-covered graphene nanosheets. The effectivity of these systems to incapacitate MDR was due to the successful combination of different aspects, including high ability of cR_{10} for nucleus targeting, strong association of DOX with nGO sheets, and a laser-triggered release of DOX and photothermal effect. $GOPR_D$ with and without laser irradiation showed the best and second best results, pointing out the critical role of cR_{10} to circumvent the MDR effect. An abrupt increase in the signal of nucleus-localized DOX and synergic photothermal and chemotherapy upon laser irradiation was a solid proof for the association of cargo and carriers even after nucleus internalization. This work introduced a newly developed, cyclic peptide-directed nucleus-translocation nanomedicine and opens a new gate to conquer MDR tumors in the future.

4. Experimental Section

Preparation of DOX-Loaded GOP and GOPR: Hydrophobic DOX was prepared based on the reported protocol.[44] GOP (20 mg) was dispersed in PBS (7.4, 20 mL), and then DOX (10 mg) dissolved in DMSO (1 mL), was added to this dispersion dropwise. The mixture was stirred overnight at room temperature and then centrifuged at 2000 rpm for 10 min. The supernatant was collected, and GOP_D was obtained after lyophilization. $GOPR_D$ was prepared with the same procedure.

The DOX loading capacity in GOP_D and $GOPR_D$ was measured by absorption at 545 nm and based on the standard curve (Figure S8, Supporting Information), which was calculated from DOX solutions (1–5 μg mL^{-1}). The following equation was employed to calculate the drug-loading capacity (DLC):

$$\text{DLC} = \frac{\text{mass of DOX in nanocarriers}}{\text{total mass of drug loaded nanocarriers}} \times 100\% \quad (1)$$

Release Profile of GOP_D and $GOPR_D$: GOP_D with 80 μg DOX content was dispersed in PBS (4 mL, pH 7.4), and then it was equally transferred into four dialysis tubes (spectra/Por MWCO 2 kD). Afterward, the tubes were immersed in four vials (2 vials contained 30 mL PBS with pH 7.4, while the other 2 vials contained 30 mL PBS with pH 5.6). Vials were set up in a thermostatic water bath (37 °C) on a heating rotator. Samples (0.1 mL) from vial medium were used for fluorescence measurements at 1 h intervals, and meanwhile, fresh PBS (0.1 mL) was replenished. One of the vials at each pH (pH 7.4 and 5.6) was irradiated with NIR laser (808 nm, 0.5 W cm^{-2}) for 5 min every 1 h. The concentration of released DOX at different time frames was determined by a microplate reader with excitation at 480 nm and emission at 550 nm, and using the calibration curve. The drug release studies were performed in triplicate. The release profiles of $GOPR_D$ were measured by the same way.

Cell Culture: All cell experiments were performed according to the German genetic engineering law and German biosafety guidelines in laboratory (level 1 biosafety). Dulbecco's modified eagle's medium (DMEM) and fetal bovine serum (FBS) were used for experiments. Multidrug-resistant human cervical tumor cells (HeLa-R cells) were received from Leibnitz Institute DSMZ—German Collection of Microorganisms and Cell Cultures. HeLa-R cells were cultured in DMEM supplemented with 10% (v/v) FBS and 1% penicillin-streptomycin at 37 °C with 5% CO_2 in a humidified atmosphere. Additionally, DOX.HCl (0.5 μg mL^{-1}) was added in the medium during the incubation to maintain their drug-resistance.

CCK-8 Assay: HeLa-R cells (5×10^3 cells per well) were seeded in 96-well plates with 100 μL DMEM and cultured for another 24 h before the biocompatibility and antitumor tests.

GOP and GOPR were dissolved in the culture medium and then added to the HeLa-R cell with a series of concentrations (from 1 to 500 μg mL^{-1}), respectively. The culture medium solutions were removed after 24 h incubation, and the wells were rinsed with PBS. Afterward, medium-containing CCK-8 (100 μL, 10%) was added to each well. After a 2 h incubation, the absorbance of each well at 450 nm was measured. Cells without any treatments were considered as a negative control, and the cytotoxicity of DOX.HCl (2 and 50 μg mL^{-1}) was measured in the same way as the positive controls. Each test was triplicated.

The antitumor tests for GOP_D and $GOPR_D$ were performed by almost the same procedure. However, the concentration of DOX was changed from 0.01 to 100 μg mL^{-1}. The tests were replicated as 2 groups, and NIR laser irradiation (808 nm, 0.5 W cm^{-2}) was employed to one group for 10 min after 6 h incubation.

Confocal Laser Scanning Microscopy: HeLa-R cells were seeded in 8-well plates with the density of 3×10^4 cells per well and incubated for another 24 h before CLSM experiments. Cellular uptake of GOP and GOPR: GOP_F and $GOPR_F$ were dispersed in DMEM (20 μg mL^{-1}) and incubated with the cells at 37 °C for 1, 3, and 6 h, respectively. Subsequently, the wells were rinsed with PBS, and then the nucleus of HeLa-R cells was stained with Hoechst for 30 min. Afterward, cells were observed with CLSM (Leica TCS SP8). Hoechst was excited at 350 nm with the emission at 460 nm, and FITC was excited at 488 nm with the emission at 520 nm. Intracellular DOX release: DOX.HCl, GOP_D, and $GOPR_D$ were dispersed in DMEM and then added to the wells. The concentration of DOX for all experiments was set at 5 μg mL^{-1}. Each experiment was replicated as two groups, and the cell culture medium was refreshed after 6 h incubation. Subsequently, one group was treated with NIR laser irradiation (808 nm, 0.5 W cm^{-2}) for 10 min, while the other group was not treated and used as control. Afterward, the cells were incubated with the fresh medium for additional 6 h. Finally, cells were rinsed with PBS and the nucleus was stained with Hoechst before evaluation by CLSM. Hoechst was excited at 350 nm with the emission at 460 nm, and DOX was excited at 488 nm with the emission at 550 nm.

Flow Cytometer: HeLa-R cells were seeded in 24-well plates (5×10^4 cells per well), and they were incubated for 24 h before experiments. Cellular uptake of GOP and GOPR: GOP_F and $GOPR_F$ were dispersed in DMEM (20 μg mL^{-1}) and then added to the cells. The cells were incubated with GOP_F and $GOPR_F$ for 6 h before rinsing with PBS. Then the cells were treated with trypsin/EDTA for 4 min and centrifuged at 1000 rpm, and the supernatant was discarded. Cells were re-suspended in PBS, and fluorescence was measured (excitation: 488 nm; emission: 520 nm) using a BD FACS caliber flow cytometer. Intracellular DOX release: DOX.HCl, GOP_D, and $GOPR_D$ were dispersed in DMEM and

then added to the cells. The concentration of DOX for all experiments was set at 5 μg mL^{-1}, and all of the experiments were replicated as two groups. One group was treated with NIR laser irradiation (808 nm, 0.5 W cm^{-2}) for 10 min after 6 h incubation while the other group was not treated and used as control. Afterward, the cells were incubated with fresh medium for another 6 h before rinsing with PBS. Then the cells were treated with trypsin/EDTA and centrifuged to discard the supernatant. Cells were re-suspended in PBS, and fluorescence was measured (excitation: 488 nm; emission: 550 nm) using a BD FACS caliber flow cytometer.

Tumor Xenograft Models on Nude Mice: Female BALB/c nude mice (4 weeks old) were purchased from Model Animal Research Center of Nanjing University (Nanjing, China), and all animal experiments were conducted in compliance with the National Institute of Health Guide for the Care and Use of Laboratory Animals (China). 1×10^6 HeLa-R cells were subcutaneously inoculated into the right flank of one nude mouse to construct the tumor-bearing mice. Tumor size was measured by electronic caliper, and the tumor volume (V) was calculated as $V = a^2 \times b/2$ (a and b represent the width and length of the tumor, respectively). And the body weight of nude mice was recorded by an electronic balance.

In Vivo Photothermal Studies: HeLa-R tumor-bearing nude mice were intravenously injected with saline, DOX.HCl, GOP_D, and $GOPR_D$ (5 mg kg^{-1}). After 24 h, the tumor sites were irradiated by NIR laser (808 nm, 0.5 W cm^{-2}) for 10 min, and the thermal photos were recorded by an IR thermal imaging camera (FLIR, E40) during the irradiation every 2 min.

In Vivo Biodistribution Studies: For the quantitative drug distribution experiments, HeLa-R tumor-bearing nude mice were intravenously administrated with GOP_D and $GOPR_D$ (5 mg kg^{-1}). After 24 h, the mice were sacrificed, and the organs were extracted and homogenized in 1 mL 1% Triton X-100. Extracting solution (HCl-IPA, 5 mL) was added to tissue lysates and the samples were kept at 4 °C overnight. After that, the mixture was centrifuged at 11000 rpm for 15 min. The concentration of DOX was determined by the fluorescence measurement of the supernatant.

In Vivo Antitumor Efficacy: When the tumor volume reached about 100 mm^3, the nude mice were randomly divided into 6 groups with 6 mice in one group. Then the mice were intravenously administrated with saline (group 1), DOX.HCl (group 2), $GOPR_D$ (group 3), GOPR (group 4), GOP_D (group 5), and $GOPR_D$ (group 6). The ratio of DOX amount and body weight was 5 mg kg^{-1}. After 24 h, the tumors in groups 1, 2, 4, 5, and 6 were irradiated with NIR laser (808 nm, 0.5 W cm^{-2}) for 10 min. The tumor size and body weight were recorded every 2 days during the treatment. The mice were sacrificed after 16 days, and then the tumors and major organs were isolated and stained by hematoxylin & eosin (H&E). In addition, Ki67 and TUNEL immunostaining were also applied for all of the tumors.

Supporting Information

Supporting Information is available from the Wiley Online Library or from the author.

Acknowledgements

R.H. acknowledges Focus Area Nanoscale of Freie Universität Berlin and SFB 765 for the financial support. W.C. would like to thank the National Natural Science Foundation of China (NSFC 51703244 and 51973233), the Natural Science Foundation of Jiangsu Province (BK20170730), and the Jiangsu Specially-Appointed Professor Program. C.P.R.H. acknowledges support from the SFB 765 and the SPP 1623 (Deutsche Forschungsgemeinschaft). H.Q. appreciates the Fundamental Research Funds for the Central Universities (2632020ZD13). The financial support from Iran Science Elites Federation and China Scholarship Council (CSC) was acknowledged. The authors thank Dr. J. Radnik and Ms. Eng. J. Stockmann (BAM) for running XPS on the studied samples. The authors would like to appreciate Dr. Pamela Winchester for proofreading the manuscript. R. Volkmer and I. Kretzschmar are acknowledged for the synthesis of cyclic R10 peptides.

Conflict of Interest

The authors declare no conflict of interest.

Keywords

cyclic cell penetrating peptide, graphene oxide, multidrug resistance, nuclear targeting, synergistic therapy

Received: January 31, 2020
Revised: May 14, 2020
Published online:

[1] R. L. Siegel, K. D. Miller, A. Jemal, *Ca-Cancer J. Clin.* **2020**, *70*, 7.
[2] R. Sullivan, O. I. Alatise, B. O. Anderson, R. Audisio, P. Autier, A. Aggarwal, C. Balch, M. F. Brennan, A. Dare, A. D'Cruz, *Lancet Oncol.* **2015**, *16*, 1193.
[3] J. Liu, M. Li, Z. Luo, L. Dai, X. Guo, K. Cai, *Nano Today* **2017**, *15*, 56.
[4] T. Reiss, K. Hjelt, A. C. Ferrari, *Nat. Nanotechnol.* **2019**, *14*, 907.
[5] G. Reina, J. M. González-Domínguez, A. Criado, E. Vázquez, A. Bianco, M. Prato, *Chem. Soc. Rev.* **2017**, *46*, 4400.
[6] Z. Tu, G. Guday, M. Adeli, R. Haag, *Adv. Mater.* **2018**, *30*, 1706709.
[7] A. Assali, O. Akhavan, M. Adeli, S. Razzazan, R. Dinarvand, S. Zanganeh, M. Solaimani, M. Dinarvand, F. Atyabi, *Nanomed.: Nanotechnol., Biol. Med.* **2018**, *14*, 1891.
[8] Y.-W. Chen, Y.-L. Su, S.-H. Hu, S.-Y. Chen, *Adv. Drug Delivery Rev.* **2016**, *105*, 190.
[9] K. Yang, L. Feng, Z. Liu, *Adv. Drug Delivery Rev.* **2016**, *105*, 228.
[10] S. Suryaprakash, M. Li, Y. H. Lao, H. X. Wang, K. W. Leong, *Carbon* **2018**, *129*, 863.
[11] R. Kurapati, S. P. Mukherjee, C. Martín, G. Bepete, E. Vazquez, A. Pénicaud, B. Fadeel, A. Bianco, *Angew. Chem., Int. Ed.* **2018**, *57*, 11722.
[12] N. Lu, L. Wang, M. Lv, Z. Tang, C. Fan, *Nano Res.* **2019**, *12*, 247.
[13] K. H. Tan, S. Sattari, I. S. Donskyi, J. L. Cuellar-Camacho, C. Cheng, K. Schwibbert, A. Lippitz, W. E. S. Unger, A. Gorbushina, M. Adeli, *Nanoscale* **2018**, *10*, 9525.
[14] Z. Chen, T. Shi, L. Zhang, P. Zhu, M. Deng, C. Huang, T. Hu, L. Jiang, J. Li, *Cancer Lett.* **2016**, *370*, 153.
[15] a) Z. Tu, H. Qiao, Y. Yan, G. Guday, W. Chen, M. Adeli, R. Haag, *Angew. Chem., Int. Ed. Engl.* **2018**, *57*, 11198; b) Z. Tu, H. Qiao, Y. Yan, G. Guday, W. Chen, M. Adeli, R. Haag, *Angew. Chem.* **2018**, *130*, 11368.
[16] M. Chen, X. Liang, C. Gao, R. Zhao, N. Zhang, S. Wang, W. Chen, B. Zhao, J. Wang, Z. Dai, *ACS Nano* **2018**, *12*, 7312.
[17] Y. Zhong, J. Zhang, R. Cheng, C. Deng, F. Meng, F. Xie, Z. Zhong, *J. Controlled Release* **2015**, *205*, 144.
[18] L. Zhao, Y.-H. Xu, T. Akasaka, S. Abe, N. Komatsu, F. Watari, X. Chen, *Biomaterials* **2014**, *35*, 5393.
[19] D. Zhong, Z. Tu, X. Zhang, Y. Li, X. Xu, Z. Gu, *Biomacromolecules* **2017**, *18*, 3498.
[20] L. Pan, J. Liu, J. Shi, *Chem. Soc. Rev.* **2018**, *47*, 6930.

[21] L. Pan, Q. He, J. Liu, Y. Chen, M. Ma, L. Zhang, J. Shi, *J. Am. Chem. Soc.* **2012**, *134*, 5722.
[22] L. Pan, J. Liu, Q. He, J. Shi, *Adv. Mater.* **2014**, *26*, 6742.
[23] Z. Yu, W. Pan, N. Li, B. Tang, *Chem. Sci.* **2016**, *7*, 4237.
[24] N. Li, Q. Sun, Z. Yu, X. Gao, W. Pan, X. Wan, B. Tang, *ACS Nano* **2018**, *12*, 5197.
[25] S. Han, Z. Li, J. Zhu, K. Han, Z. Zeng, W. Hong, W. Li, H. Jia, Y. Liu, R. Zhuo, *Small* **2015**, *11*, 2543.
[26] W. Jiang, J. Wang, J. Yang, Z. He, Z. Hou, Y. Luo, L. Wang, J. Liu, H. Zhang, Y. Zhao, *Nano Res.* **2018**, *11*, 5716.
[27] W. Gao, X. Yang, Z. Lin, B. He, D. Mei, D. Wang, H. Zhang, H. Zhang, W. Dai, X. Wang, *J. Controlled Release* **2017**, *261*, 174.
[28] D. Mandal, A. N. Shirazi, K. Parang, *Angew. Chem., Int. Ed.* **2011**, *50*, 9633.
[29] G. Lättig-Tünnemann, M. Prinz, D. Hoffmann, J. Behlke, C. Palm-Apergi, I. Morano, H. D. Herce, M. C. Cardoso, *Nat. Commun.* **2011**, *2*, 453.
[30] N. Nischan, H. D. Herce, F. Natale, N. Bohlke, N. Budisa, M. C. Cardoso, C. P. R. Hackenberger, *Angew. Chem., Int. Ed.* **2015**, *54*, 1950.
[31] F. F. Hilário, M. D. M. Traoré, V. Zwick, L. Berry, C. A. Simões-Pires, M. Cuendet, N. Fantozzi, R. P. de Freitas, M. Maynadier, S. Wein, *Org. Lett.* **2017**, *19*, 612.
[32] a) H. D. Herce, D. Schumacher, A. F. L. Schneider, A. K. Ludwig, F. A. Mann, M. Fillies, M.-A. Kasper, S. Reinke, E. Krause, H. Leonhardt, *Nat. Chem.* **2017**, *9*, 762; b) A. F. L. Schneider, A. L. D. Wallabregue, L. Franz, C. P. R. Hackenberger, *Bioconjugate Chem.* **2019**, *30*, 400.
[33] E. A. Nigg, *Nature* **1997**, *386*, 779.
[34] K. Weis, *Cell* **2003**, *112*, 441.
[35] Y. Chong, C. Ge, G. Fang, X. Tian, X. Ma, T. Wen, W. G. Wamer, C. Chen, Z. Chai, J.-J. Yin, *ACS Nano* **2016**, *10*, 8690.
[36] M. J. Sweetman, S. M. Hickey, D. A. Brooks, J. D. Hayball, S. E. Plush, *Adv. Funct. Mater.* **2019**, *29*, 1808740.
[37] S. Abbina, S. Vappala, P. Kumar, E. M. J. Siren, C. C. La, U. Abbasi, D. E. Brooks, J. N. Kizhakkedathu, *J. Mater. Chem. B* **2017**, *5*, 9249.
[38] F. Yoshino, T. Amano, Y. Zou, J. Xu, F. Kimura, Y. Furusho, T. Chano, T. Murakami, L. Zhao, N. Komatsu, *Small* **2019**, *15*, 1901930.
[39] M. F. Gholami, D. Lauster, K. Ludwig, J. Storm, B. Ziem, N. Severin, C. Böttcher, J. P. Rabe, A. Herrmann, M. Adeli, *Adv. Funct. Mater.* **2017**, *27*, 1606477.
[40] Z. Tu, K. Achazi, A. Schulz, R. Mülhaupt, S. Thierbach, E. Rühl, M. Adeli, R. Haag, *Adv. Funct. Mater.* **2017**, *27*, 1701837.
[41] Y. Hou, L. Yu, M. Zhang, W. Xie, J. L. Cuellar-Camacho, Z. Chu, Q. Wei, R. Haag, *Nano Lett.* **2020**, *20*, 748.
[42] P. Dey, S. Hemmati-Sadeghi, R. Haag, *Polym. Chem.* **2016**, *7*, 375.
[43] H. Tian, T. P. Sakmar, T. Huber, *Chem. Commun.* **2016**, *52*, 5451.
[44] Z. Tu, V. Wycisk, C. Cheng, W. Chen, M. Adeli, R. Haag, *Nanoscale* **2017**, *9*, 18931.
[45] X. Ke, V. W. L. Ng, R. J. Ono, J. M. W. Chan, S. Krishnamurthy, Y. Wang, J. L. Hedrick, Y. Y. Yang, *J. Controlled Release* **2014**, *193*, 9.
[46] Z. Gu, S. Zhu, L. Yan, F. Zhao, Y. Zhao, *Adv. Mater.* **2019**, *31*, 1800662.
[47] Y. Su, T. Yu, W. Chiang, H. Chiu, C. Chang, C. Chiang, S. Hu, *Adv. Funct. Mater.* **2017**, *27*, 1700056.
[48] T. Yin, J. Liu, Z. Zhao, Y. Zhao, L. Dong, M. Yang, J. Zhou, M. Huo, *Adv. Funct. Mater.* **2017**, *27*, 1604620.
[49] N. Kamaly, B. Yameen, J. Wu, O. C. Farokhzad, *Chem. Rev.* **2016**, *116*, 2602.
[50] Y. Zhang, X. Zhu, X. Chen, Q. Chen, W. Zhou, Q. Guo, Y. Lu, C. Li, Y. Zhang, D. Liang, *Adv. Funct. Mater.* **2019**, *29*, 1806620.
[51] K. Yang, Y. Li, X. Tan, R. Peng, Z. Liu, *Small* **2013**, *9*, 1492.
[52] D.-X. Ye, Y.-Y. Ma, W. Zhao, H.-M. Cao, J.-L. Kong, H.-M. Xiong, H. Möhwald, *ACS Nano* **2016**, *10*, 4294.
[53] F. Liu, L. Lin, Y. Zhang, Y. Wang, S. Sheng, C. Xu, H. Tian, X. Chen, *Adv. Mater.* **2019**, *31*, 1902885.
[54] L. Wu, X. Cai, H. Zhu, J. Li, D. Shi, D. Su, D. Yue, Z. Gu, *Adv. Funct. Mater.* **2018**, *28*, 1804324.
[55] C. Zhang, W.-L. Liu, X.-F. Bai, S.-X. Cheng, Z.-L. Zhong, X.-Z. Zhang, *Biomaterials* **2019**, *199*, 1.